Thermodynamic Properties of Potassium Oxide (K₂O) Nanoparticles by Molecular Dynamics Simulations

V. Guder* and S. Senturk Dalgic

Trakya University, Faculty of Science, Department of Physics, Balkan Campus, 22030 Edirne, Turkey

Potassium oxide (K_2O) is a reagent for testing the presence of other compounds in chemical reactions. It is also used in compounding cement and in glass making. However properties of K_2O in nanoscale are still unclear. In this work, thermodynamic properties of spherical K_2O nanoparticles have been investigated. Size dependent cohesive energy, melting point and glass transition temperature have been computed for different sizes of K_2O nanoparticles by molecular dynamics simulations. Thermal expansion coefficients of nanoparticles at zero pressure and various temperatures have been also calculated. Melting point depression for K_2O nanoparticles was determined. The significant change in cohesive energy was obtained for particles smaller than 5.4 nm. The presented model is successful in understanding the size-dependent thermodynamics of spherical K_2O nanoparticles. Theoretical investigations of the thermal properties of K_2O nanoparticles have not been presented previously.

1. Introduction

Little experimental work has been focused on K_2O. Recent computational experiments have done little to add to the existing data. K_2O crystallizes into a stable face-centered cubic antifluorite (anti CaF_2) structure (space group Fm−3m) at room temperature [1]. In recent years, fluorites and antifluorites have an increased interest of researchers due to their high temperature properties. Dovesi et al. [2] have calculated the lattice constants and elastic properties of K_2O using the ab initio Hartree-Fock LCAO method at zero pressure. Cancarevic et al. [3] have studied the stability and solid phase transition of K_2O under pressure using LCAO method. Zhuravlev et al. [4] and Eithiraj and co-workers [5] have discussed electronic band structure of K_2O using the self consistent pseudopotential method (PP) and tight-binding linear muffin-tin orbitals (TB-LMTO), respectively. Moakafi et al. [6] have investigated structural, electronic and optical properties of K_2O at normal conditions and under pressure using FPAPW+LO method. Zhuravlev et al. [7] have observed transformation into hexagonal phase of K_2O at a temperature above 645 K. The first purpose of the present work is to investigate the structural solid phase transition of K_2O under higher temperature. In this work three different solid phase transitions of K_2O were observed at 850 K, 1300 K and 1350 K. However, theoretical investigations of the thermal properties of K_2O nanoparticles have not been presented previously and properties of K_2O at the nanoscale level are still unclear. The second aim is to investigate thermodynamic properties and the size dependence of melting temperature of K_2O nanoparticles. We use the open source code LAMMPS MD

simulator, which can be run in massively parallel environments and provide efficient simulation on metal atomic scale systems [8] and GULP (General Utility Lattice Program) [9].

2. Materials and methods

Two-body ionic short range interaction Born-Mayer potentials formed by combination of the Buckingham and a long range Coulomb interaction terms [10] is given by

$$E_{ij} = A_{ij} \exp\left(-\frac{r_{ij}}{\rho_{ij}}\right) - \frac{C_{ij}}{r_{ij}^6} + \frac{q_i q_j}{r_{ij}}, \tag{1}$$

where r_{ij} is the distance between ions i and j, with charges q_i and q_j, and A_{ij}, ρ_{ij} and C_{ij} are fitting parameters. Lattice energy minimization was performed using both GULP and LAMMPS simulation codes at 0 K and 0 GPa. However all molecular dynamic simulations during heating of K_2O were performed using only LAMMPS. Simulations of K_2O have adopted three dimensional periodic boundary conditions using the Ewald sum method for long distance interactions and have processed the integration of motion equations by velocity-verlet algorithm. The constant number of particles, pressure and temperature ensemble, as (NPT) for bulk system, and the constant number of particles, volume and temperature ensemble, as (NVT) for nanoparticles system, were simulated. Nose-Hoover barostat was used to control the pressure and temperature. The integration step was 0.001 ps with the velocity given by Maxwell distribution. The value of Born Mayer type potential cut off diameter was 5.5 Å. Anti-CaF_2 type bulk K_2O cubic simulation cells, $8 \times 8 \times 8$, repeated periodically in space group Fm-3m, had contained 6144 atoms. Anti-$PbCl_2$ type bulk K_2O orthorhombic simulation cells, $6 \times 6 \times 7$, repeated periodically in space group Pnam, had contained 6048 atoms. Anti-CdI_2 type bulk K_2O hexagonal simulation cell, $13 \times 13 \times 13$, repeated periodically in space group P-3m1, had contained 6591 atoms. Anti-$CdCl_2$ type bulk

---

*corresponding author; e-mail: vildanguder@hotmail.com

K_2O hexagonal simulation cell, $9 \times 9 \times 9$, repeated periodically in space group R-3m, had contained 6561 atoms. The initial structure was given by random functions, followed by a heating process, ranging from 0 to 2500 K with the temperature interval of 50 K and a relaxation time of 100 ps for all structures.

3. Results and discussion

The reliability of the values for interatomic potentials were determined by computer simulations study, using interaction potentials. The potential parameters used in the MD simulations were obtained from the binks.lib force field libraries [11] of GULP. The K_2O potential parameters are listed in Table I. For atoms of K and O, the q values are $+1$ and -2, respectively.

TABLE I

Potential parameters for K_2O.

Buckingham	A_{ij} [eV]	ρ [Å]	C_{ij} [eV A^6]
K-K	2189.190	0.1916	0.0
K-O	958.210	0.3606	0.0
O-O	9547.960	0.2192	32.0

Understanding the anisotropic elastic behaviour of tissues is important for the calculation of accurate elastic constants of anti-CaF$_2$-type K_2O. Table II, shows the calculated values of lattice constant, lattice energy, density, bulk modulus and elastic constants (C_{11}, C_{12}, C_{44}) for anti-CaF$_2$-type K_2O, together with the experimental and other data. Lattice constant and energy calculation was performed using both GULP and LAMMPS simulation codes at 0 K and 0 GPa.

TABLE II

Structure optimization results of anti-CaF$_2$-type K_2O.

	GULP	LAMMPS	Exp.	Other
a [Å]	6.437	6.436	6.436[1]	
E [kJ/mol]	2187.978	2188.371	2232.1[12]	
ρ [g/cm^3]	2.345		2.32[13]	
Bulk modulus [GPa]	40.119			40.74[3], 38.92[3]
$C_{11} = C_{22} = C_{33}$ [GPa]	73.407			89.0[14]
$C_{12} = C_{13} = C_{23}$ [GPa]	23.475			20.2[14]
$C_{44} = C_{55} = C_{66}$ [GPa]	22.345			13.1[14]

The calculated ground state total energy as a function of lattice parameter is plotted in Fig. 1 for anti-CaF$_2$ type K_2O along with Brich-Murnaghan fit. The equilibrium lattice parameter can be clearly seen from figure as 6.436 Å for anti-CaF$_2$ structure, which is equal to experimental value of 6.436 Å [1].

The dependence of total lattice energy on simulation time of K_2O in the structure of anti-CaF$_2$, anti-PbCl$_2$, anti-CdCl$_2$ and anti-CdI$_2$ is illustrated in Fig. 2a–d, respectively. The total lattice energy fluctuates around
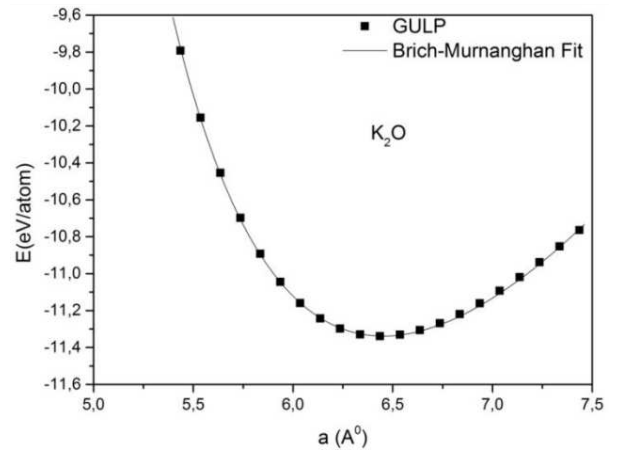

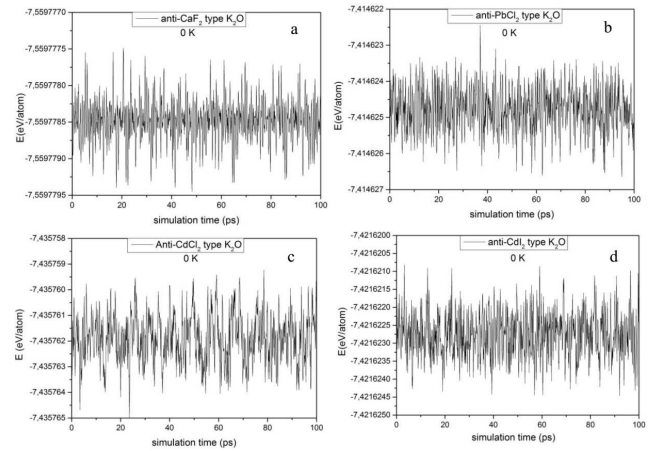Fig. 1. The total lattice energy of anti-CaF$_2$ type K_2O, as a function of the lattice parameter.

Fig. 2. The dependence of total lattice energy as a function of simulation time for (a) anti-CaF$_2$, (b) anti-PbCl$_2$, (c) anti-CdCl$_2$ and (d) anti-CdI$_2$-type K_2O at 0 K.

a defined value. Although the amplitude of these fluctuations is large, the exchange energy decreases with simulation time. This means that once the system reaches a metastable state it transits to a more stable state, that is, energy change is very small. The relaxation is continued until system reaches equilibrium state.

Figure 2a shows that the total energy has oscillated around -7.5597785 eV/atom and the change in total energy is maximum 0.000002 eV/atom during the duration of the entire simulation time for anti-CaF$_2$-type K_2O.

Figure 2b shows that the total energy has oscillated around -7.41462464 eV/atom and the change in total energy is maximum 0.000004 eV/atom during the duration of the entire simulation time for anti-PbCl$_2$-type K_2O.

Figure 2c shows that the total energy has oscillated around -7.43576186 eV/atom and the change in total energy was maximum 0.000005 eV/atom for anti-CdCl$_2$-type K_2O.

Figure 2d shows that the total energy has oscillated around -7.42162275 eV/atom and the change in total energy was maximum 0.000003 eV/atom during the simulation time for anti-CdI$_2$-type K$_2$O. As a result, the entire system has reached equilibrium at 100 ps.
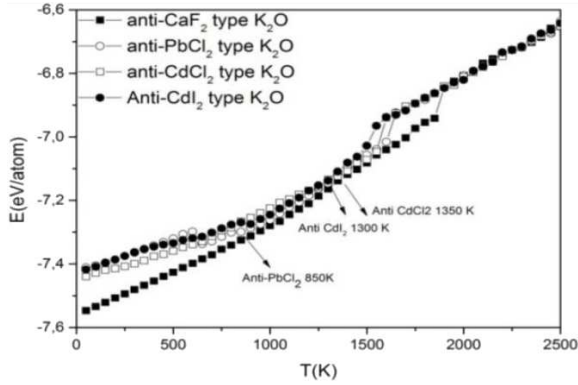

Fig. 3. The temperature dependence of total lattice energy for anti-CaF$_2$, anti-PbCl$_2$, anti-CdCl$_2$ and anti-CdI$_2$-type K$_2$O, during heating process.

K$_2$O can form different crystal structures, such as anti-CaF$_2$, anti-PbCl$_2$, anti-CdCl$_2$ and anti-CdI$_2$. We have compared the energies of all these mentioned phases. The most stable structure for bulk K$_2$O is anti-CaF$_2$, because this structure has the lowest energy. Figure 3 shows the temperature dependence of total energy for anti-CaF$_2$, anti-PbCl$_2$, anti-CdCl$_2$ and anti-CdI$_2$-type K$_2$O, during heating process.

It can be seen from Fig. 3 that total energy of anti-CaF$_2$ type K$_2$O has the same value as the energy of anti-PbCl$_2$, anti-CdI$_2$ and anti-CdCl$_2$-type bulk K$_2$O, at temperatures of 850 K, 1300 K and 1350 K, which means presence of phase transformation to anti-CaF$_2$ type from anti-PbCl$_2$, anti-CdI$_2$ and anti-CdCl$_2$-type bulk K$_2$O.

The total energy changes slope at ~ 1100 K, which means an appearance of solid to solid phase transition of bulk K$_2$O. It has been observed that at a temperature above 1100 K, stable structure of bulk K$_2$O is disrupted and undergoes a transition to the other phase from anti-CaF$_2$ phase. In this work we were unable to determine the other phase.

The total lattice energy and heat capacity, as a function of temperature for K$_2$O in anti-CaF$_2$, anti-PbCl$_2$, anti-CdCl$_2$ and anti-CdI$_2$ structure are given in Fig. 4a–d, respectively. Figure 4a shows, that total energy and heat capacity sharply increase at 1850 K, which means an appearance of melting for anti-CaF$_2$-type K$_2$O.

Figure 4b shows that total energy and heat capacity sharply decrease at 600 K, which means an appearance of solid to solid phase transition, which starts at 600 K but is completed at 850 K for anti-PbCl$_2$-type K$_2$O. Besides, the total energy and heat capacity have sharp increase at 1600 K which means an appearance of melting for anti-PbCl$_2$-type K$_2$O.
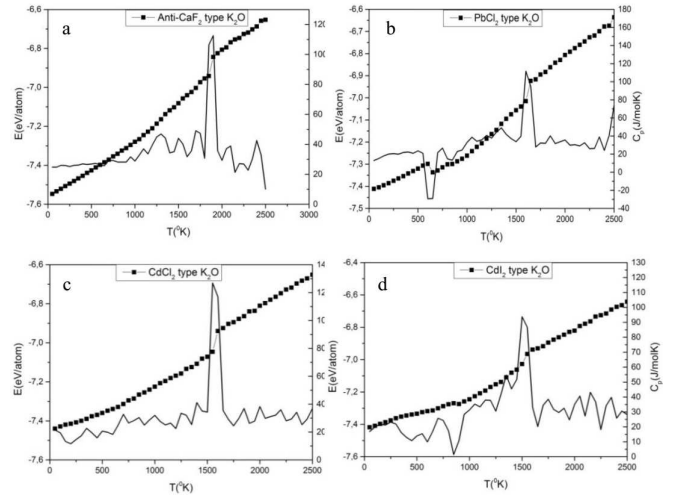

Fig. 4. Temperature dependence of total lattice energy and heat capacity for (a) anti-CaF$_2$, (b) anti-PbCl$_2$, (c) anti-CdCl$_2$ and (d) anti-CdI$_2$-type K$_2$O, during heating process.

Figure 4c shows that total energy and heat capacity sharply increase at 1550 K, which means presence of melting point for anti-CdCl$_2$-type K$_2$O.

Figure 4d shows that total energy and heat capacity sharply decrease at 850 K, which shows presence of solid to solid phase transition, starting at 850 K, but completed at 1300 K for anti-CdI$_2$-type K$_2$O. Besides, total energy and heat capacity sharply increase at 1500 K, which means presence of melting point at this temperature in anti-CdI$_2$-type K$_2$O.
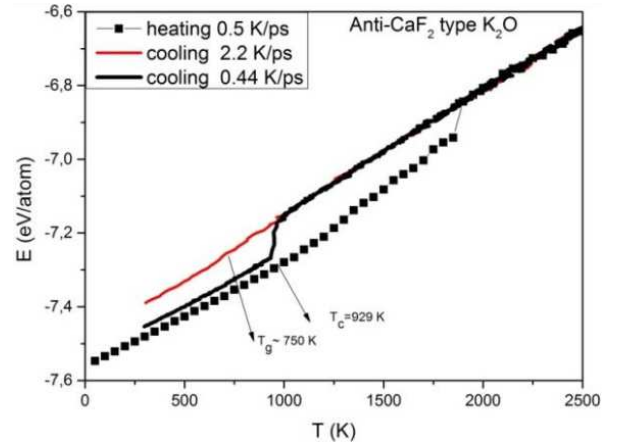

Fig. 5. The temperature dependence of total lattice energy of anti-CaF$_2$ bulk K$_2$O at heating and cooling processes.

We have considered three cooling rates, to investigate the effect of cooling rate on the glass transition temperature T_g and crystallization temperature T_c. Figure 5 shows the temperature dependence of total lattice energy of anti-CaF$_2$-type K$_2$O, for the heating rate of $\gamma = 0.5$ K/ps and for the cooling rates of $\gamma = 0.44$ K/ps,

$\gamma = 2.2$ K/ps. The total energy curves above the melting temperature almost overlap for the different cooling rates. This shows that the atoms can move rapidly enough, according to the temperature change. The total energy drops linearly with the decreasing temperature. However, when the temperature decreases below 970 K, the total energy change shows different cooling rate. This indicates the formation of a crystallization and metallic glass.

It is observed that the total energy changes have big breaks at about 929 K with decreasing temperature, for the the cooling rate of $\gamma = 0.44$ K/ps. This break shows that liquid to crystallized phase transition occurs. When the system is cooled to 929 K with the cooling rate of 2.2 K/ps, we still observe the structure of liquid, in fact a supercooled region. Actually the system is in the crystalline state during heating process at the same temperature. Liquid in the region between the point of broken energy curve during cooling process and melting temperature corresponds to so-called supercooled liquid. The energy curve slope at ~ 750 K, with the cooling rate of 2.2 K/ps, shows that metallic glass transition occurs.
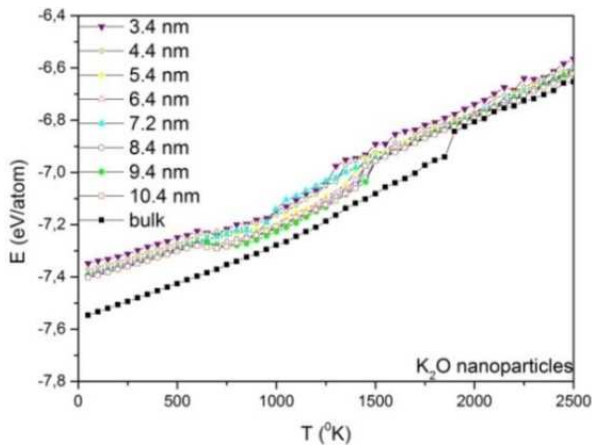

Fig. 6. Temperature dependence of the total energy of K₂O nanoparticles.

We can discuss the results of MD simulations performed to study the effect of the size (diameter) of nanoparticles on melting points. Temperature dependence of total energies of K₂O nanoparticles of different diameters is plotted in Fig. 6. From figure, it can be recognized that the solid-solid phase transition range of K₂O nanoparticles is within $700 - 850$ K and melting range is within $1300 - 1550$ K. As the diameter of nanoparticles is increased, the overall melting temperatures of nanoparticles is increased. Because of the surface energies, total energies of nanoparticles are higher than those of bulk, and their energies get closer to the value of bulk, as the diameter of nanoparticles is increased. There is a visible change in energy of nanaporticles smaller than 5.4 nm in diameter, but there is no visible change in energy of nanoparticles larger than 5.4 nm in indiameter, caused by the approach to the bulk value.

MD simulation images have been observed at different temperatures in order to define the atomic structure through the melting process. When temperature increases, bonds between atoms become weak, there is a conversion to an irregular structure from a regular structure and a phase transition occurs. Figure 7a shows structure of complete K₂O nanoparticle with the diameter of 5.4 nm at 300 K, in the solid phase and with a stable structure.
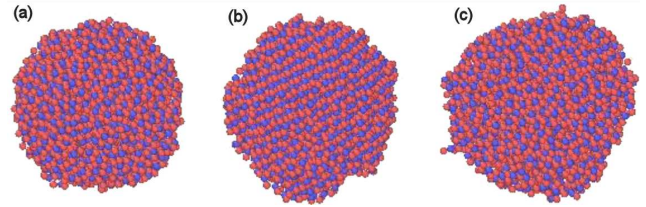

Fig. 7. Snapshots of the K₂O nanoparticles with the diameter of 5.4 nm at (a) 300 K, (b) 950 K, (c) 1500 K.

When the temperature increases up to 950 K, atoms are placed into new lattice points and the system changes to another solid phase (Fig 7b). Figure 7c shows that it becomes liquid at 1500 K and that it is completely melted.
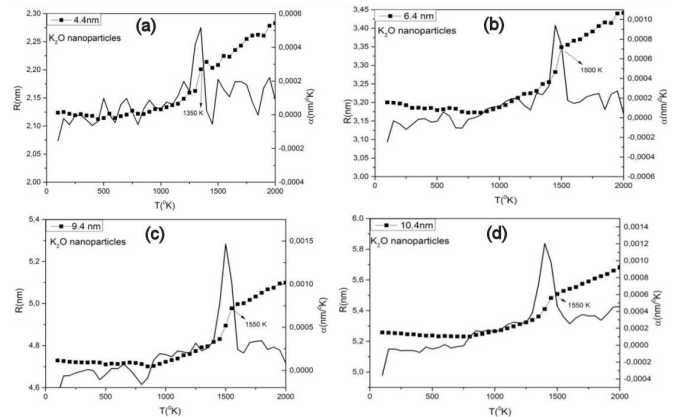

Fig. 8. The temperature dependence of radius and thermal expansion coefficients for the diameters of 4.4 nm, 6.4 nm, 9.4 nm and 10.4 nm of K₂O nanoparticles.

Figure 8 shows that there are three distinct region of radius-temperature curve. As the temperature increases, radius of nanoparticles decreases until the solid solid phase transition is reached. After phase transition has occurred, radius of nanoparticles increases. At melting, it also shows a sharp increase. The total energy sharply increases at temperatures of 1350 K, 1500 K, 1550 K and 1550 K respectively, which means appearance of K₂O liquid with the diameter of 4.4 nm, 6.4 nm, 9.4 nm and 10.4 nm. As the dimension approaches bulk limit, the system becomes liquid at the same temperature for 9.4 nm and 10.4 nm

4. Conclusions

The melting and phase transition evolution of K_2O, in stable anti-CaF_2 structure is investigated by the molecular dynamics simulation using Born–Mayer potential. We have modeled the atomic structure of bulk K_2O using different structural optimization methods. The calculated values of the lattice constant, bulk modulus, elastic constants and cohesive energy are in reasonable agreement with experimental measurements and with previous theoretical data. We have observed transformation to cubic phase stable anti-CaF_2 from orthorhombic phase anti-$PbCl_2$, hexagonal phase anti-CdI_2 and anti-$CdCl_2$, at 850 K, 1300 K and 1350 K, respectively, for bulk K_2O. It has been observed that at a temperature above 1100 K, stable structure of bulk K_2O is disrupted and undergoes a transition to another phase from anti-CaF_2 phase, in bulk K_2O. The melting point obtained from the MD simulations is T_m = 1850 K, 1600 K, 1550 K and 1500 K for anti-CaF_2, anti-$PbCl_2$, anti-$CdCl_2$ and anti-CdI_2-type, respectively, in bulk K_2O. We show that, melting temperatures of K_2O nanoparticles are lower than those of bulk K_2O and decrease with the reducing diameter, in nanoscale regime. The Born–Mayer type potential is successfully used for understanding the liquid structure of K_2O and the size dependent thermodynamic properties of spherical K_2O nanoparticles.

Acknowledgments

References

[1] E. Zintl, A. Harder, B. Dauth, *Zeitschrift für Elektrochemie und angewandte physikalische Chemie* **40**, 588 (1934).

[2] R. Dovesi, C. Roetti, C. Freyria-Fara, M. Prencipe, V.R. Saunders, *Chem. Phys.* **156**, 11 (1991).

[3] Z. Cancarevic, J.C. Schön, M. Jansen, *Phys. Rev. B* **73**, 224114 (2006).

[4] Y.N. Zhuravlev, Y.M. Basalaev, A.S. Poplavnoi, *Russ. Phys. J.* **44**, 398 (2001).

[5] R.D. Eithiraj, G. Jaiganesh, G. Kalpana, *Phys. B* **396**, 124 (2007).

[6] M. Moakafi, R. Khenata, A. Bouhemadou, H. Khachai, B. Amrani, D. Rached, M. Rerat, *Eur. Phys. J. B* **64**, 35 (2008).

[7] Yu.N. Zhuravlev, D.V. Korabel'nikov, M.V. Aleinikova, *Phys. Solid State* **54**, 1518 (2012).

[8] S. Plimpton, *J. Comp. Phys.* **117**, 1 (1995).

[9] J.D. Gale, A.L. Rohl, *Mol. Simul.* **29**, 291 (2003).

[10] P.P. Ewald, *Ann. Phys.* **64**, 253 (1921).

[11] D.J. Binks, Ph.D. Thesis, Surrey University, 1994.

[12] A. Melillou, B.R.K. Gupta, *Czechoslovak J. Phys.* **41**, 813 (1991).

[13] chemister.ru/Database/properties-en.php?dbid=1&id=516.

[14] Yu.N. Zhuravlev, O.S. Obolonskaya, *J. Struct. Chem.* **51**, 1005 (2010).